SUPPLEMENTAL INFORMATION

SUPPLEMENTAL FIGURES

Figure S1 (related to Figure 1).

Comparison of *Nanog* reporter activities and NANOG expression in early blastocysts.

(A) Schematic of FACS analyses (B-C) for the *Nanog:GFP*$^{Tg/+}$, *Nanog:H2B-GFP*$^{Tg/+}$, *Nanog:H2B-Venus*$^{Tg/+}$ and the *Nanog*^{GFP} targeted (TNGA) ESCs propagated after several passages in the absence of MEFs. Numbers in FACS histograms indicate percentages of GFP- (left) and GFP+ (right) populations. R1 ESCs (red histograms) were used as negative controls for calibration of GFP- and GFP+ gates. (D) Comparison of reporter activity in *Nanog:H2B-GFP*$^{Tg/+}$ESCs grown in standard serum+LIF (top panel) and 2i+LIF conditions (bottom panel). ESCs were imaged in the same imaging session with the same imaging parameters. Colonies in 2i+LIF conditions displayed markedly

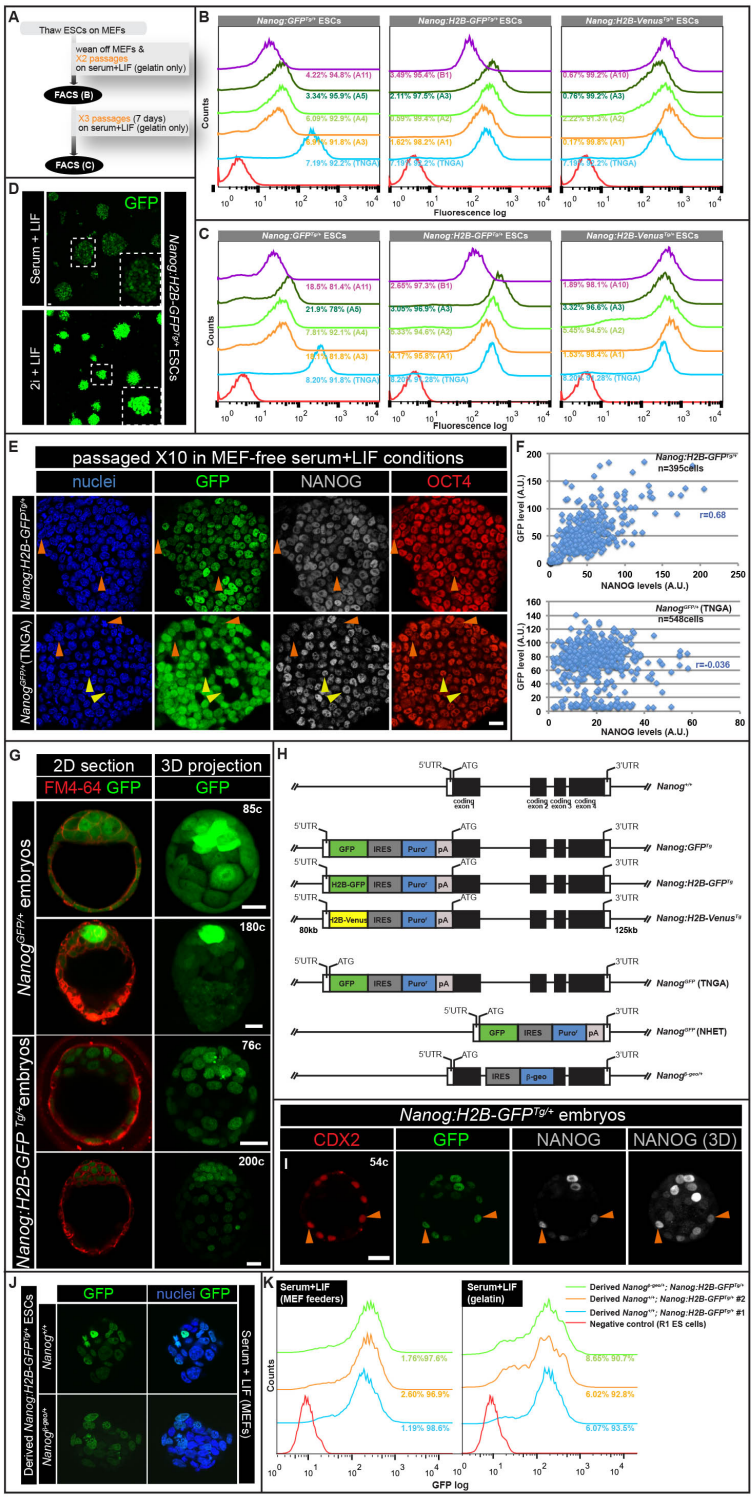

Xenopoulos *et al.*, Supplementary Figure 1 (related to Figure 1).

increased reporter activity and had a prominent round morphology, indicative of the ground state of self-renewal (Ying et al., 2008). (E) Immunostained *Nanog:H2B-GFP*$^{Tg/+}$ and TNGA ESCs after 10 passages in MEF-free serum+LIF conditions, stained for Hoechst, NANOG and OCT4. (F) Quantitative immunofluorescence after automated nuclear segmentation. Approximately 5 ESC colonies were used for the analysis, with one colony shown (E). GFP (y-axis) and NANOG (x-axis) fluorescence values plotted for individual ESCs. Cells displaying low levels of GFP, and NANOG observed within the population highlighted with orange arrowheads. In TNGA ESCs some NANOG+ GFP- cells were observed within colonies (yellow arrowheads). (G) Reporter activity in *Nanog*$^{GFP/+}$ and *Nanog:H2B-GFP*$^{Tg/+}$ blastocysts observed in live mid (~64-100 cells) and implanting (>150 cells) blastocysts stained with the membrane vital dye FM4-64. Reporter activity was elevated within the ICM. Reporter-expressing TE cells were observed in both strains. It should be noted that increased (4X) 488nm Ar laser power was used for imaging *Nanog*$^{GFP/+}$ blastocysts, due to dim reporter expression compared to *Nanog:H2B-GFP* embryos. Cell counting was carried out by staining with Hoechst for nuclear labeling. (H) Schematic of the endogenous *Nanog* locus, including the start of coding sequence (ATG), 4 coding exons, 5' and 3' UTRs. BAC-based transcriptional reporters were constructed by targeting GFP-IRES-Puro^{r}-SV40pA, H2B-GFP-IRES-Puro^{r}-SV40pA and H2B-Venus-IRES-Puro^{r}-SV40pA cassettes into the 5'UTR of the *Nanog* locus, 19bp upstream of the beginning of the ORF. The TNGA targeted allele was generated by inserting a GFP-IRES-Puro^{r}-pA cassette at the *Nanog* START (AUG) codon (Chambers et al., 2007). The *Nanog*$^{GFP/+}$ targeted allele was generated by replacing the ORF with a GFP-IRES-Puro^{r}-pA cassette (Hatano et al., 2005). The *Nanog*$^{\beta\text{-}geo/+}$ targeted allele was generated by replacing exon 2 with an IRES-β-geo cassette (Mitsui et al., 2003). (I) Immunofluorescence images of an early (54 cells) *Nanog:H2B-GFP*$^{Tg/+}$ blastocyst stained for NANOG and the TE marker CDX2. Reporter and NANOG protein expression were noted in TE cells (orange arrowheads). (J-K). Imaging and FACS analysis of embryo derived *Nanog:H2B-GFP*$^{Tg/+}$; *Nanog*$^{+/+}$ and *Nanog:H2B-GFP*$^{Tg/+}$; *Nanog*$^{\beta\text{-}geo/+}$ ESCs. ESCs were stained with Hoechst for nuclei labeling. Numbers in FACS histograms indicate percentages of GFP- (left) and GFP+ (right) populations. *r*=Pearson correlation coefficient. Scale bar: 20μm.

Figure S2 (related to Figure 2).

***Nanog:H2B-GFP* BAC transgene marks segregating EPI cells in mid blastocysts.**

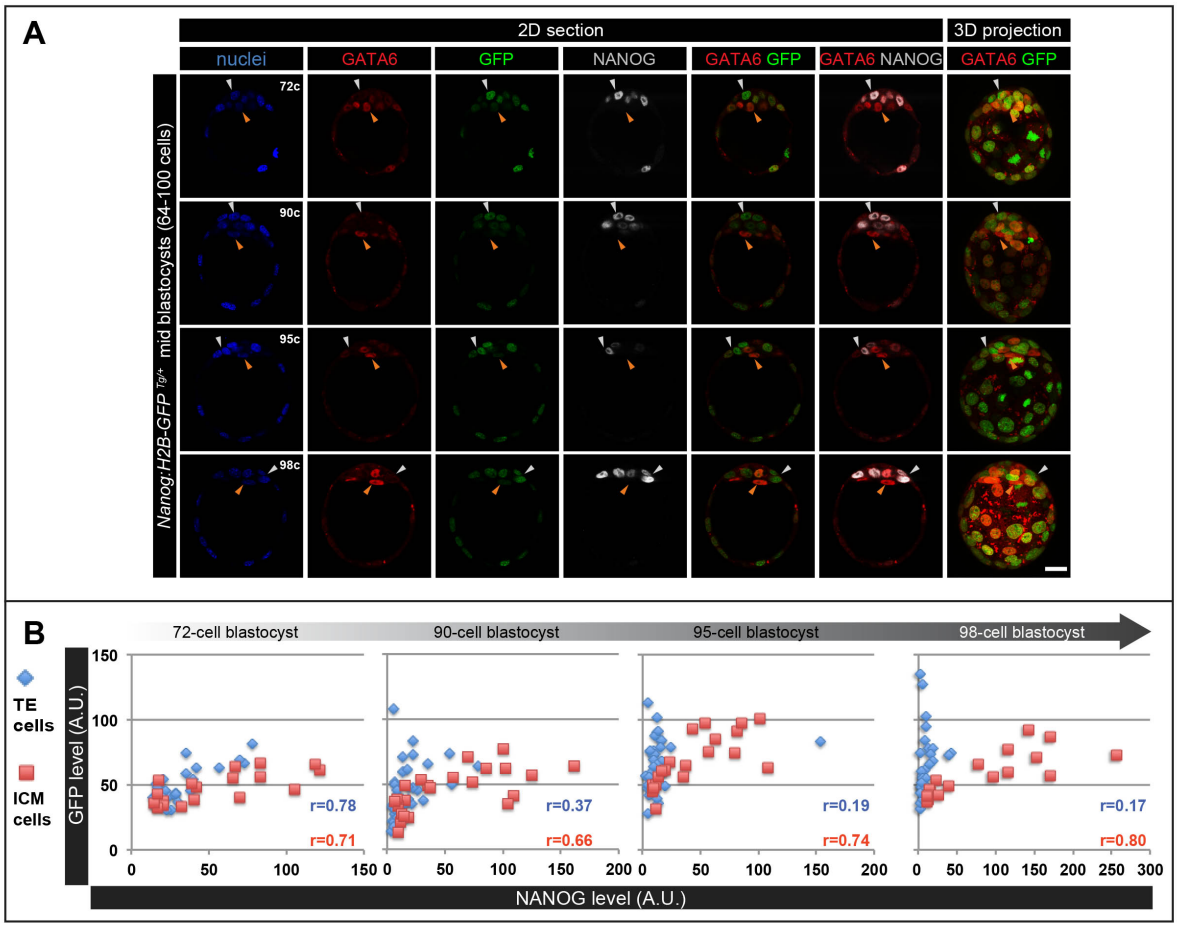

Xenopoulos *et al.*, Supplementary Figure 2 (related to Figure 2).

Nanog:H2B-GFP reporter expression in mid-blastocyst stage (~64-100 cell) embryos counterstained with Hoechst, anti-GATA6 and NANOG antibodies. (A) Embryos were imaged similarly to those in **Figure 2B**, albeit in a different imaging session and with different imaging parameters. White arrowheads identify segregating EPI-progenitors, orange arrowheads identify PrE-progenitors. (B) Quantitative immunofluorescence after MINS automated nuclear segmentation and fluorescence intensity normalization of the embryos shown in (A). Analysis was performed as in **Figure 2C**. All embryos shown were imaged with the same parameters. *R* = Pearson correlation coefficient. Scale bar: 20μm.

Figure S3 (related to Figure 3).

Modulation of FGF signaling alters *Nanog* expression distributions within the ICM.

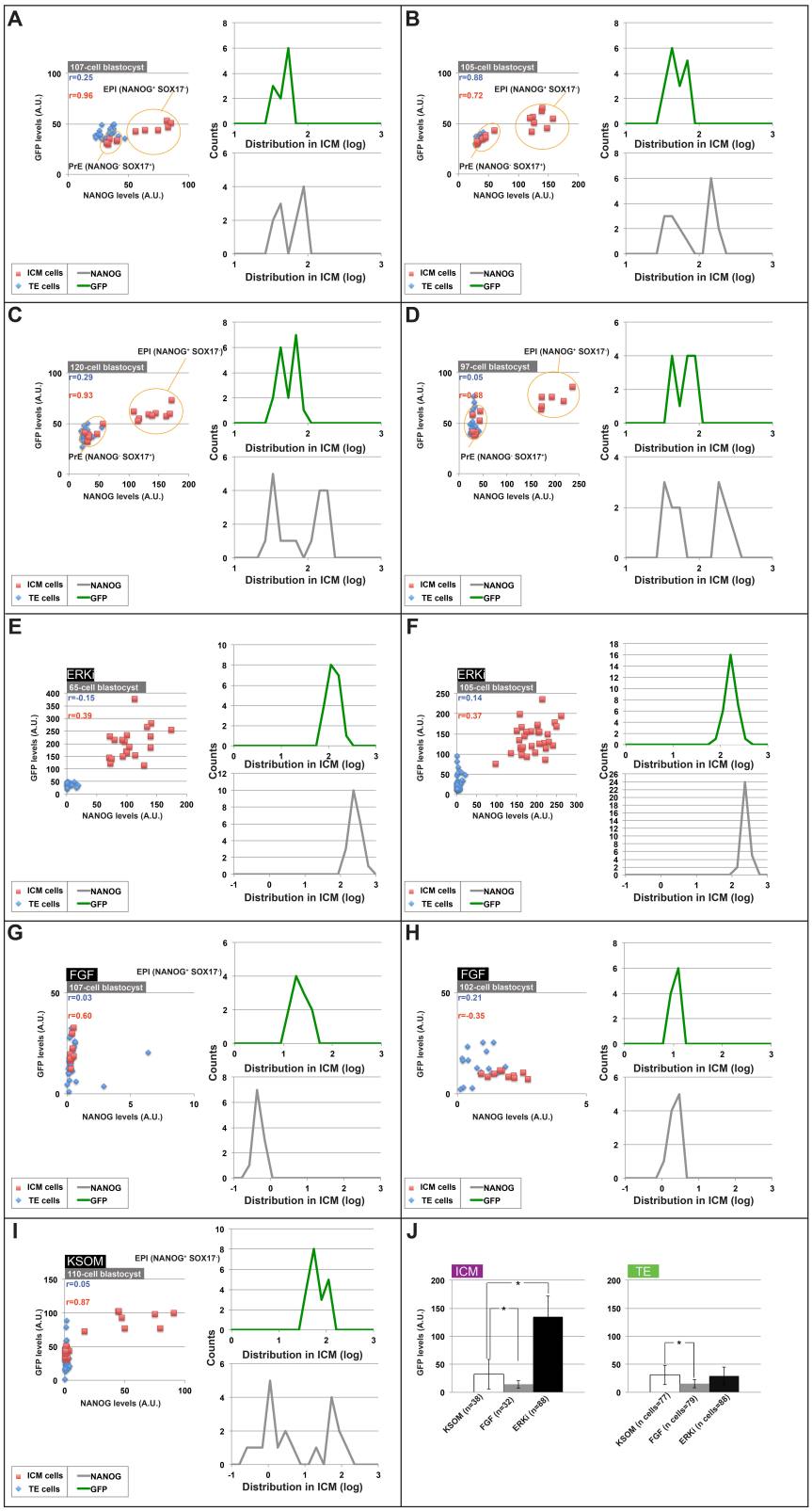

Xenopoulos *et al.*, Supplementary Figure 3 (related to Figure 3).

(A-D) Reporter and NANOG expression analyses in late (>100 cell) *Nanog:H2B-GFP*$^{Tg/+}$ blastocysts counterstained with Hoechst, anti-SOX17 and NANOG antibodies. After MINS automated nuclear segmentation, analyses were performed as shown in **Figure 3A**. Embryos in (A-B) were imaged in the same imaging session as the embryo in **Figure 3A**. Embryos in (C-D) were imaged in a different imaging session and with different imaging parameters. (E-I) Reporter and NANOG expression analyses in cultured embryos (in control KSOM medium, or medium supplemented with exogenous FGF or the ERK1/2 inhibitor PD0325901), which were imaged within the same imaging session and with

the same imaging parameters as in **Figure 3B** (all cultured embryos belonged in the same litter). After automated nuclear segmentation, analysis was performed similarly as in **Figure 3C**. Note that the x- and y-axis scales of scatter plots are different due to changes in reporter and NANOG expression in cohorts of cultured embryos. In (J) mean values for the GFP channel for ICM or TE cells were pooled from the KSOM (n=2), FGF (n=3) or ERKi (n=3) treated embryos. Error bars indicate s.d. *r* = Pearson correlation coefficient. Asterisks indicate significant differences (*P*, <0.05 by the *t* test).

Figure S4 (related to Figure 4).

Reporter activity is not diluted in dividing cells and lineage preference in the mother cell is inherited by daughter cells.

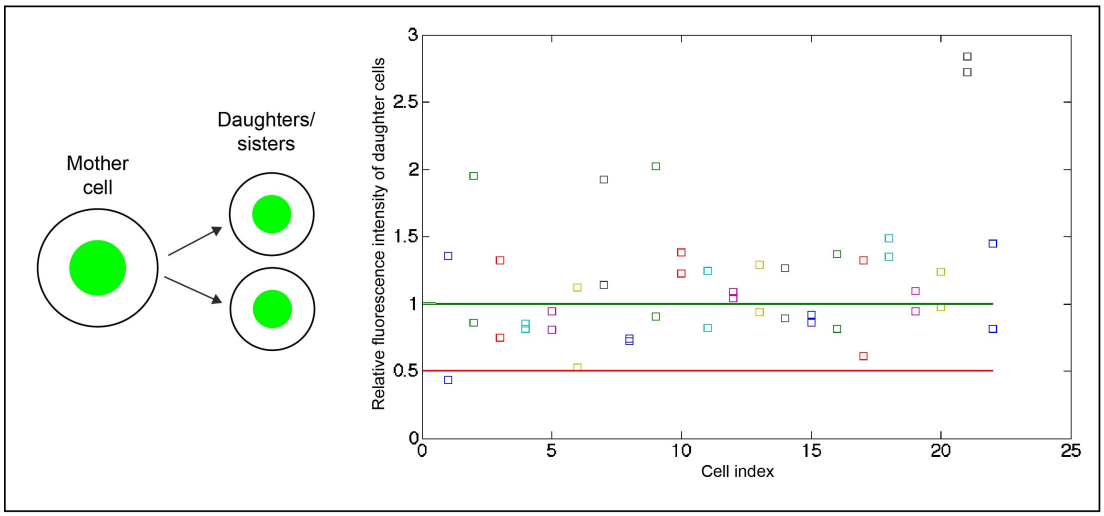

Xenopoulos *et al.*, Supplementary Figure 4 (related to Figure 4).

(A) GFP is not diluted after cell proliferation. We considered dividing EPI cells and for each track we plotted the mean fluorescence intensity value for the hour preceding, and the hour following, mitosis. We excluded bursts in fluorescence intensity due to chromosome condensation. We obtained 3 intensity values referring to mother and two daughter (i.e. sister) cells (depicted in the cartoon on the left) and plotted the relative intensity of the sisters (i.e. sister intensity/mother intensity) per each cell division (depicted on the right panel). Red and green colored continuous lines represent values of 0.5 (perfect dilution, each sister inherits one half of the total protein present in the mother cell), 1 (perfect compensation, each sister inherits the value of the mother), respectively. The average total fluorescence of sister cells slightly exceed 1 (1.16), indicating that daughter cells reached approximately the same level of fluorescence intensity as their mother cell.

Figure S5 (related to Figure 5).

Reporter expression is decreased upon exogenous FGF2 treatment, when all ICM cells commit toward the PrE lineage.

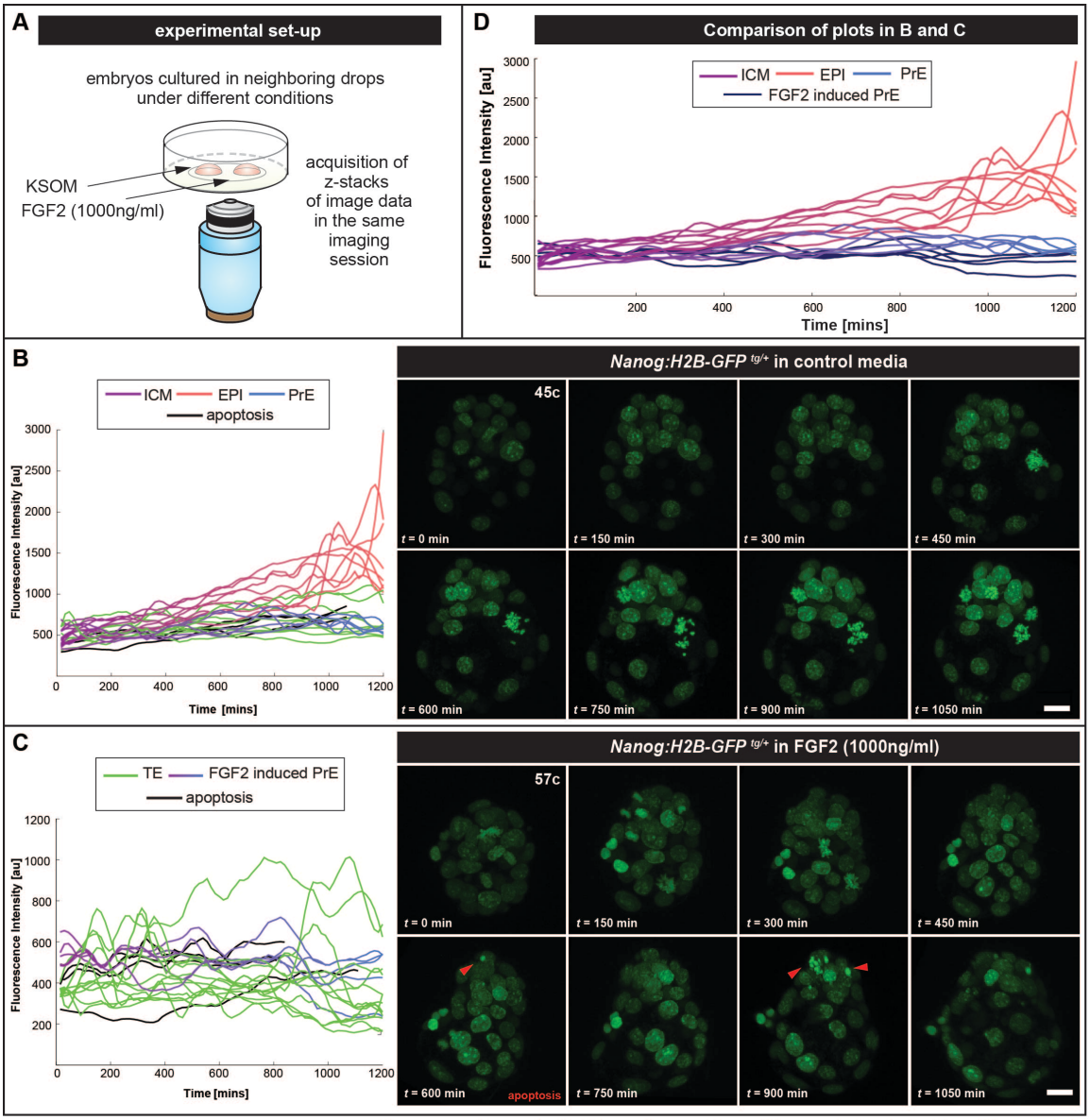

Xenopoulos *et al.*, Supplementary Figure 5 (related to Figure 5).

(A) Schematic of 3D time-lapse live imaging experiment design. Embryos cultured in different media conditions were imaged in the same session. Representative *Nanog:H2B-GFP* $^{tg/+}$ blastocysts recovered at E3.5 (comprising 45-cells, 57-cells at start of experiment/movie) and cultured *ex utero* for 1200 minutes in (B) KSOM (control media) or (C) FGF2 (1000ng/ml). Left

panels, quantification of GFP fluorescence values over time. Right panels, single time-points from 3D time-lapse movies. In control media, individual ICM cells committed to either EPI or PrE lineages, and consequently exhibited increased or decreased *Nanog:H2B-GFP* reporter activity, respectively. Under conditions of FGF treatment, all ICM cells adopted a PrE identity and exhibited a decrease in reporter activity. (D) Superimposed plot of GFP quantifications from time-lapse movies in (B) and (C) revealing decreased levels of GFP intensity in embryo cultured in the presence of FGF.

Figure S6 (related to Figure 5).

Quantitative analysis of *Nanog:H2B-GFP* reporter using cycloheximide and FGF2 suggested that half-life of H2B-GFP is less than 6 hours.

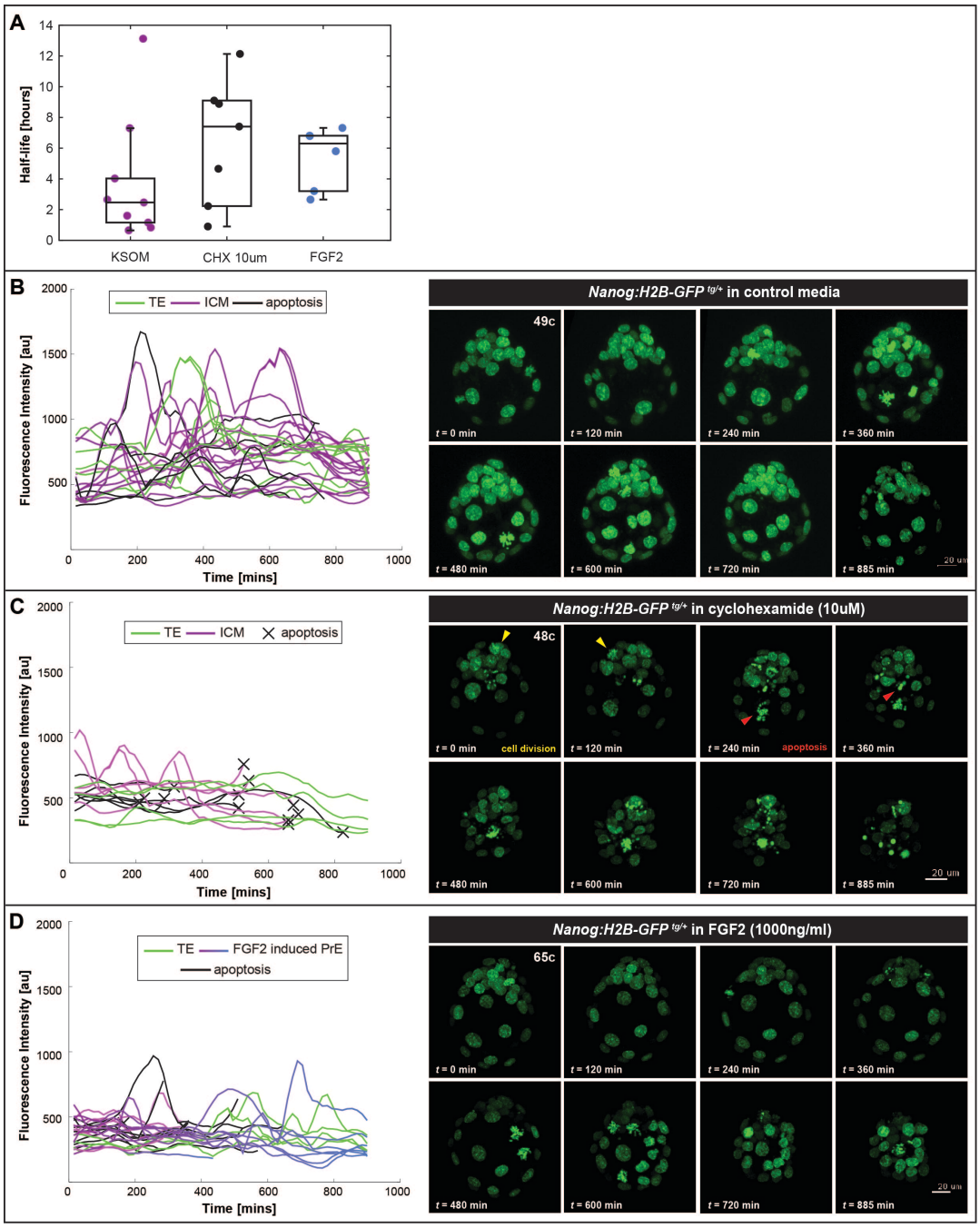

Xenopoulos *et al.*, Supplementary Figure 6 (related to Figure 5).

(A) Box plots showing the average time of half-life calculated from individual cells from 3D time-lapse movies of *Nanog:H2B-GFP* embryos in different culture conditions of (B) KSOM (control media), (C) cycloheximide (CHX, 10μM) or (D) FGF2 (1000ng/ml). Embryos cultured in different media conditions were imaged in the same session. From the movie of embryo in KSOM, only PrE cells were counted for the calculation of H2B-GFP half-life, since only those cells exhibit downregulation of reporter activity. From the movies of embryos in CHX or FGF2 treatments, both EPI and PrE-biased cells had taken into account for the calculation of H2B-GFP half-life. The mean decay rate of PrE cells from the embryo in KSOM is T = 3.8 ± 4.0 (h). The results from CHX and FGF2 treatment are T= 6.5±4.0 (h) and 5.4±2.0 (h), respectively. The higher decay rates in the condition of CHX or FGF2 are possibly due to the initial high level of fluorescence intensity in EPI-biased cells. (B-D) Quantification of GFP fluorescence values and images of single time-points from a time-lapse of *Nanog:H2B-GFP*$^{Tg/+}$ blastocysts recovered at E3.5 (comprising 49-cells, 48-cells and 65-cells at start of experiment/movie) and cultured *ex utero* in different conditions for 900 minutes. (C) Under conditions of CHX treatment, the embryo had few incidences of cell divisions, suggesting that the treatment had partially worked (yellow arrowhead). However, by the end of the movie, most of cells underwent apoptosis (red arrowhead).

SUPPLEMENTAL MOVIES

Movie S1 (related to Figures 4 and 5). Changes in GFP-positive cell distribution within the ICM of *Nanog:H2B-GFP*$^{Tg/+}$ embryos from mid to late blastocyst stages.

(A-C) 3D time-lapse movies of 3D reconstructed images of *Nanog:H2B-GFP*$^{Tg/+}$ blastocysts. (A) Embryo was collected around E3.5 (~50 cells) and cultured *ex utero* thereafter. Image data was acquired with the Zeiss LSM780 confocal system. At the end of the movie, GFP-hi cells had formed the EPI lineage, whereas GFP-low cells formed the epithelial PrE layer on the surface of the ICM. Reporter expression in the TE cells diminishes as the blastocyst develops. The embryo depicted in **Figure 4** can be seen in this movie. (B) Embryo was collected around E3.5 (54 cells) and cultured *ex utero* thereafter. Image data was acquired with the Zeiss 510 confocal system. Tracked nuclei are highlighted by dots; the outline of each dot depicts the lineage choice. Cells highlighted in red-color outlined dots are EPI progenitor cells; cells highlighted with the blue-color outlined dots are PrE progenitor cells. Movie depicts embryo in **Figure 5A**. (C) Embryo was collected around E3.75 (83 cells) and cultured *ex utero* thereafter. Image data was acquired with the Zeiss LSM510 confocal system. Tracked nuclei are highlighted as in (B). Movie depicts embryo in **Figure 5C**. For all movies, the z-section interval was 2μm and the embryos were imaged every 15min. Red arrowheads points to events of apoptosis and yellow arrowheads mark events of cell division.

Movie S2 (related to Figure 6). Changes in GFP-positive cell distribution within the ICM of a *Nanog:H2B-GFP*$^{Tg/+}$ embryo treated with an ERK inhibitor.

3D time-lapse movie of 3D reconstructed images of a *Nanog:H2B-GFP*$^{Tg/+}$ blastocyst collected around E3.5 (48-cells at start of experiment/movie) and cultured *ex utero* in the presence of the ERK inhibitor PD0325901. z-section interval was 2μm and time interval was 15min. At the end of the movie, the majority of the ICM consisted of GFP-hi cells that had acquired an EPI identity. Yellow arrowheads mark cell divisions in EPI-specified cells. Movie depicts embryo in **Figure 6**.

SUPPLEMENTAL RESULTS

Extracting *Nanog* transcriptional dynamics from *Nanog:H2B-GFP* reporter. To study the dynamics of *Nanog* transcription, we used a reporter construct in which the promoter of *Nanog* drives expression of H2B-GFP. This construct has the advantage of providing information on *Nanog* transcription as well as allowing single cell resolution and tracking. In this Section, we use a computational approach to estimate how the dynamics of H2B-GFP relates to the dynamics of *Nanog* transcription.

(i) *H2B-GFP dilution*. Cell proliferation demands that an increasing number of H2B molecules are incorporated in nuclei. Depending on the amount of free H2B molecules in the cytoplasm, cell division could cause a dilution of histone molecules. We found that $NANOG^+$ EPI cells proliferate significantly more than $NANOG^-$ PrE cells, suggesting that the dilution of H2B-GFP does not contribute significantly to the observed differentiation dynamics. To further verify whether we could detect a dilution of H2B-GFP signal we focused on dividing EPI cells. We found no evidence for dilution of H2B-GFP (**Figure S4**). Collectively, our observations imply that H2B dilution does not affect our measurements of *Nanog* transcriptional dynamics.

(ii) *H2B-GFP half-life*. Histones can be long-lived molecules. It is, therefore, important to understand how the lifetime of H2B-GFP might affect the measurements of *Nanog* transcriptional dynamics in the pre-implantation embryo. To this end, we first estimated experimentally an upper bound for the half-life of H2B-GFP, using three independent approaches. First, we treated embryos with cycloheximide (to inhibit protein translation) and measured the decay of H2B-GFP (**Figure S6**). High concentrations of cycloheximide are toxic and causes massive and rapid cell death in embryos. We, therefore, used a relatively low concentration (10μM), which causes a partial inhibition of protein translation, as exemplified by the fact that we still observe cell divisions, which require protein translation. Estimating a half-life of H2B-GFP using an exponential decay fit, therefore, gives us an upper bound on the half-life of H2B-GFP. We find such upper bound to be 6.5±4 hours. We also repeated similar analysis for embryos treated with FGF4 (**Figure S5**). In such embryos, all cells assume the PrE fate and downregulated *Nanog* expression. From the measurements of the decay of H2B-GFP, we obtain an upper bound for H2B-GFP half-life of 5.4±2 hours, compatible with the estimate from

the cycloheximide experiment (**Figure S6**). Finally, we use the decay of the fluorescence traces from PrE cells, in which a clear and sharp decrease of H2B-GFP fluorescence is observed at the onset of cell differentiation (**Figure S6**). Assuming that the production of NANOG rapidly switch from an on to an off state at the time of differentiation, we can fit the decay of the fluorescence signal with an exponential decay and extrapolate an upper bound for H2B-GFP. Performing this analysis on several cells provides the value 3.8±4 hours. Collectively, these experiments allow us to conclude that the half-life of H2B-GFP is shorter than 6 hours and, in fact, not very dissimilar for NANOG half-life, which is about 4 hours (Abranches et al., 2013).

To determine which changes in *Nanog* transcription can be effectively tracked with a reporter of half-life of few hours, we used a mathematical model that describes the dynamics of H2B-GFP:

$ds/dt=a(t)-s/t-s/t_1$

$ds^*/dt=s/t-s^*/t_1$

where a(t) is H2B-GFP production rate, s is the amount of immature H2B-GFP, s* is the amount of fluorescent H2B-GFP, t is the maturation rate of GFP and t_1 is the lifetime of H2B-GFP. Estimate of t suggest that it is of the order of 30 minutes, implying that GFP maturation is much faster than the timescales of interest. We, therefore, assume that s is always close to steady state. The equations above reduce to:

$ds^*/dt=b(t)-s^*/t_1$

where $b(t)=a(t)t_1/(t+t_1)$.

Next, we needed to estimate the amount of noise in the detection of *Nanog:H2B-GFP* reporter activity. To this end, we performed filtering on the traces of non-dividing EPI traces to remove small (time) scale fluctuations but keep slow dynamics. Filtering was achieved by smoothing on the scale of 2.5h. Noise was then estimated by calculating the mean deviation of the original signal from the filtered signal. We obtained an estimate of about 6% of average *Nanog* expression levels in EPI cells. Assuming that we can reliably measure changes in gene expression that are above two-fold of the level of noise, we conclude that changes in gene expression which are two-folds or higher and persists for at least 2 hours can be reliably tracked. Collectively, this analysis shows that our transcriptional reporter allows us to follow the transcriptional dynamics of *Nanog* in pre-implantation embryos with temporal resolution of less than 2 hours. Such resolution is sufficient for our studies of cell differentiation dynamics, which happens on much longer timescales (10-15 hours) (Leveau and Lindow, 2001).

SUPPLEMENTAL EXPERIMENTAL PROCEDURES

Generation of reporter constructs by BAC modification.

BAC clone RP23-117I23 (CHORI, BACPAC Resources) containing the *Nanog* gene, was modified using RED/ET recombination [GeneBridges; (Angrand et al., 1999)] as described previously (Okita et al., 2007). Reporter cassettes were generated by ligating GFP-IRES-Puro^r, H2B-GFP-IRES-Puro^r and H2B-Venus-IRES-Puro^r fragments with a PGK-Hygro-FRT cassette (GeneBridges). The *Nanog* 5'UTR was targeted (19bp upstream of the beginning of the ORF) by attaching homology arms to both ends of reporter cassettes by PCR amplification using the following 50bp oligos: NanogGFP-Fw (5'-TTTGCATTAGACATTTAACTCTTCTTTCTATGATCTTTCCTTCTAGACACGCCACCATGGTGAGCAAGGGCGAG-3'), NanogH2B-Fw (5'- (5'-TTTGCATTAGACATTTAACTCTTCTTTCTATGATCTTTCCTTCTAGACACGCCACCATGCCAGAGCCAGCG-3') and NanogpIRESpuro3-R (5'-GCGAGGGAAGGGATTTCTGAAAAGGTTTTAGGCAACAACCAAAAAACTCACGCCAAGCTCTAGCTAGAGGTCGACG-3'). The underlined sequences depict the homology arms for the *Nanog* 5'UTR, which are the same as used previously (Okita et al., 2007).

Generation of transgenic mESCs and mice.

Transgenic mESCs were generated by nucleofection (Amaxa, Lonza) of R1 ESCs (Nagy et al., 1993) with 10μg of undigested modified BAC DNA purified with the large-construct kit (Qiagen). After 4 days 1.5μg/ml puromycin selection was started. Resistant colonies were picked after 10 days of selection. Clonal lines were expanded and propagated in the presence or absence of mouse embryonic fibroblasts (MEFs). At least two ESC clones for each reporter were analyzed. Transgenic mice were generated by pronuclear injection of undigested modified BAC carrying the *Nanog:H2B-GFP* cassette purified with the large-construct kit (Qiagen). The BAC construct was injected into F1XF1 zygotes by the Memorial Sloan Kettering Mouse Genetics Core Facility following standard protocols (Nagy, 2003.). Founder animals were identified by PCR. Amplification generated a 475bp fragment from the GFP cassette using primers IMR872 Fw: AAGTTCATCTGCACCACCG and IMR873 Rev: TGCTCAGGTAGTGGTTGTCG. Four transgenic founder lines, #32, #38, #40 and #105, were established each exhibiting a similar pattern and level of reporter expression. Only one line (#38) is presented here in detail. The

transgene exhibited Mendelian inheritance, stable transgene activity and comparable levels of reporter expression within litters and across generations. Animals homozygous for the transgene were viable and fertile; only embryos heterozygous for the transgene were characterized in this study. Mice were maintained in accordance with National Institute of Health guidelines for the care and use of laboratory animals and under the approval of the MSKCC Institutional Animal Care and Use Committee.

Embryo collection and *in vitro* culture.

Embryos were recovered in M2 (Millipore) and cultured in KSOM (Millipore) medium as described previously (Kang et al., 2013). For FGF incubation experiments, FGF2 (R&D systems) at concentrations of 1000 ng/mL, supplemented with 1 μg/mL heparin (Sigma) was added to KSOM medium. For incubation experiments with an ERK1/2 inhibitor and cycloheximide, 1μM PD0325901 (StemGent) and 10μM cycloheximide (Sigma-Aldrich) were added to KSOM medium. Staining of live embryos with the vital dye FM4-64 (Invitrogen), was carried out as described previously (Plusa et al., 2008). Late morulae (~16-32 cell embryos) with or without zona pellucidae were cultured in micro-drops (10 embryos/15 μL drop) under mineral oil for 36 hours.

ESC culture.

Cell lines used in this study were *Nanog:GFP*$^{Tg/+}$, *Nanog:H2B-GFP*$^{Tg/+}$ and *Nanog:H2B-Venus*$^{Tg/+}$ transgenic R1 ESCs, targeted *Nanog*$^{GFP/+}$-clone A ESCs (TNGA) (Chambers et al., 2007) and embryo derived *Nanog:H2B-GFP*$^{Tg/+}$; *Nanog*$^{+/+}$ or *Nanog:H2B-GFP*$^{Tg/+}$; *Nanog*$^{tm1-geo/+}$ ESCs. ESCs were thawed on mouse embryonic fibroblast (MEF) feeder layers in medium containing high glucose Dulbecco's modified Eagle's medium (D-MEM, Gibco) supplemented with 15% fetal bovine serum (FBS), 0.1 mM 2-mercaptoethanol, 1 mM non-essential amino acids, 1 mM sodium pyruvate, 2 mM glutamine, 100 units/mL penicillin and 100 μg/mL streptomycin and recombinant leukemia inhibitory factor (LIF). ESCs were propagated routinely on gelatin in the absence of feeders. ESCs were cultured on gelatin in 2i (ESGRO, Millipore, supplemented with 1μM PD0325901 and 3μM Chiron, StemGent) and LIF.

FACS analysis and cell sorting.

ESCs were prepared for FACS analysis and sorting using a FACSCalibur (BD Biosciences) and MoFlo (Dako) high-speed cell sorter and analyzer respectively by harvesting cells in 0.025% trypsin/EDTA (Invitrogen) followed by neutralization of trypsin in growth medium. Live single cell populations were selected for further analyses based on Forward Scatter (FSC) and Side Scatter (SSC) characteristics, as well cell viability evaluations using Propidium Iodide (PI) staining. Parental R1 ESCs were used as a negative non-fluorescent control (Nagy et al., 1993). Cells with fluorescence levels (GFP, H2B-GFP or H2B-Venus) within this range were considered to be negative. Histograms of the FACS data were generated using FlowJo (Tree Star, Inc).

ESC cell derivation from embryos.

ESCs were derived from *Nanog:H2B-GFP*$^{Tg/+}$; *Nanog*$^{+/+}$ or *Nanog:H2B-GFP*$^{Tg/+}$; *Nanog*$^{tm1-geo/+}$ blastocysts as described previously (Czechanski et al., 2014). Newly derived ESC lines were gradually weaned off 2i, and propagated in standard serum + LIF conditions in the presence or absence of MEFs.

Image data acquisition and processing.

512 X 512 pixel images were acquired on Zeiss LSM510 META or LSM700 laser scanning confocal microscopes. Fluorescence was excited with a 405-nm laser diode (Hoechst), a 488-nm Argon laser (GFP), a 543-nm HeNe laser (Alexa-Fluor-543/555) and a 633-nm HeNe laser (Alexa-Fluor-633/647 or FM4-64). Images were acquired using a 40X objective, with optical section thickness of 0.5μm for ESCs and 1μm for embryos. Raw data were processed using ZEN software (Carl Zeiss Microsystems). For any given experiment, all ESC and embryo images were obtained with the same image acquisition parameters (laser intensity, gain, pinhole size).

Fluorescence Intensity Normalization using Robust Curve Fitting

Assuming that the true intensities of the Hoechst channel are consistent throughout the depth of view, we used a robust curve fitting technique to model the intensity attenuation as a function of the depth *Z* (see **Figure 2A**). Specifically, we used a generalized logistic function as the underlying model because the observed data points exhibited a strong S shape. The fitting

process serves the purpose of model parameter estimation. In particular, it optimizes the sum of squared loss between observed points and their estimates using unconstrained nonlinear optimization. In MATLAB, unconstrained nonlinear optimization can be implemented using the function 'fminsearch'. However, two issues may cause the fitting result problematic. Firstly, 'fminsearch' is prone to local minimum because of the non-convexity of the objective function. Also, outlier data points may severely deteriorate the fitting result. To overcome these issues we incorporated two additional techniques. Firstly, we used multiple randomized initializations. Secondly, we applied the RANdom SAmple Consensus (RANSAC) algorithm to make curve fitting robust towards outliers.

Cell tracking

To track cells even in the presence of extensive drift, either of cohorts of cells within the embryo or of the entire embryo, we used PIV tracking (Raffel, 1998). For each plane of a given segmented cell this algorithm seeks the best match in the next frame in terms of cross correlation between successive fluorescence images. The median over the planes is then taken as the cell index in the next frame. Among the untracked cells, around 20-30% of cells were dividing or undergoing apoptosis and were manually tracked, while for others their fluorescence signal was unclear as they were at the very top or bottom of the z-stack, or were incorrectly segmented. To correct for whole-embryo drift we calculated the embryo's center of mass and subtracted the motion of the embryo from the individual cell trajectories. Fluorescence signal was corrected for changes in penetration along axial position. The intensity profile along the z direction of all segmented nuclei was fitted with a linear function, and the obtained correction factor was used to correct fluorescence intensities at each time point. Time traces of fluorescence intensities were filtered using Savitzky-Golay polynomial fitting with order 3 and length 7 (i.e. around 50 minutes forward and backward). Of note, an increase in fluorescence emitted from the *Nanog:H2B-GFP* transgene was routinely observed during mitosis, due to chromosome condensation; the resulting rapid oscillations in reporter activity were not considered to be caused by changes in gene expression. Tracking scripts were written in MATLAB (http://katlab-tools.org/). Data were numerically analyzed with the open source software package GNU Octave.

SUPPLEMENTAL REFERENCES

Abranches, E., Bekman, E., and Henrique, D. (2013). Generation and characterization of a novel mouse embryonic stem cell line with a dynamic reporter of Nanog expression. PLoS One *8*, e59928.

Angrand, P.O., Daigle, N., van der Hoeven, F., Scholer, H.R., and Stewart, A.F. (1999). Simplified generation of targeting constructs using ET recombination. Nucleic acids research *27*, e16.

Chambers, I., Silva, J., Colby, D., Nichols, J., Nijmeijer, B., Robertson, M., Vrana, J., Jones, K., Grotewold, L., and Smith, A. (2007). Nanog safeguards pluripotency and mediates germline development. Nature *450*, 1230-1234.

Czechanski, A., Byers, C., Greenstein, I., Schrode, N., Donahue, L.R., Hadjantonakis, A.K., and Reinholdt, L.G. (2014). Derivation and characterization of mouse embryonic stem cells from permissive and nonpermissive strains. Nat Protoc *9*, 559-574.

Hatano, S.Y., Tada, M., Kimura, H., Yamaguchi, S., Kono, T., Nakano, T., Suemori, H., Nakatsuji, N., and Tada, T. (2005). Pluripotential competence of cells associated with Nanog activity. Mech Dev *122*, 67-79.

Kang, M., Piliszek, A., Artus, J., and Hadjantonakis, A.K. (2013). FGF4 is required for lineage restriction and salt-and-pepper distribution of primitive endoderm factors but not their initial expression in the mouse. Development *140*, 267-279.

Leveau, J.H., and Lindow, S.E. (2001). Predictive and interpretive simulation of green fluorescent protein expression in reporter bacteria. J Bacteriol *183*, 6752-6762.

Mitsui, K., Tokuzawa, Y., Itoh, H., Segawa, K., Murakami, M., Takahashi, K., Maruyama, M., Maeda, M., and Yamanaka, S. (2003). The homeoprotein Nanog is required for maintenance of pluripotency in mouse epiblast and ES cells. Cell *113*, 631-642.

Nagy, A., Gertsenstein, M., Vintersten, K., and Behringer, R. (2003.). Manipulating the mouse embryo: a laboratory manual. Cold Spring Harbor Laboratory Press, Cold Spring Harbor, New York.

Nagy, A., Rossant, J., Nagy, R., Abramow-Newerly, W., and Roder, J.C. (1993). Derivation of completely cell culture-derived mice from early-passage embryonic stem cells. Proc Natl Acad Sci U S A *90*, 8424-8428.

Okita, K., Ichisaka, T., and Yamanaka, S. (2007). Generation of germline-competent induced pluripotent stem cells. Nature *448*, 313-317.

Plusa, B., Piliszek, A., Frankenberg, S., Artus, J., and Hadjantonakis, A.K. (2008). Distinct sequential cell behaviours direct primitive endoderm formation in the mouse blastocyst. Development *135*, 3081-3091.

Raffel, M., Willert, C.E., and Kompenhans, J. (1998). Particle Image Velocimetry: A Practical Guide. Springer, Berlin.

Ying, Q.L., Wray, J., Nichols, J., Batlle-Morera, L., Doble, B., Woodgett, J., Cohen, P., and Smith, A. (2008). The ground state of embryonic stem cell self-renewal. Nature *453*, 519-523.